Vibration-mediated Kondo effect in a single-molecule quantum dot coupled to ferromagnetic electrodes

2008 J. Phys.: Condens. Matter 20 045219

(http://iopscience.iop.org/0953-8984/20/4/045219)

IOP PUBLISHING JOURNAL OF PHYSICS: CONDENSED MATTER

J. Phys.: Condens. Matter **20** (2008) 045219 (8pp) doi:10.1088/0953-8984/20/04/045219

Vibration-mediated Kondo effect in a single-molecule quantum dot coupled to ferromagnetic electrodes

Rui-Qiang Wang, Yun-Qing Zhou and D Y Xing

National Laboratory of Solid State Microstructures and Department of Physics, Nanjing University, Nanjing 210093, People's Republic of China

Received 22 September 2007, in final form 6 November 2007
Published 8 January 2008
Online at stacks.iop.org/JPhysCM/20/045219

Abstract

The nonequilibrium Green's function approach and canonical transformation technique are applied to spin-polarized electron transport through a single-molecule quantum dot connected to two ferromagnetic leads in the Kondo regime. A joint effect of electron–electron interactions with finite U and electron–phonon interaction (EPI) leads to a zero-bias anomaly of tunneling magnetoresistance (TMR), the phonon-enhanced negative zero-bias TMR being closer to its experimental value. An effective exchange field on the dot in parallel alignment of magnetizations results in an EPI-dependent splitting of the Kondo peak and EPI-dependent shifts of Kondo satellites. The strong Franck–Condon blockade due to molecule vibrations is also discussed.

1. Introduction

Recently, the single-molecule quantum dot has been proposed as a promising candidate for functional elements due to the miniaturization of electronic devices. The single-molecule device has a number of interesting features, which are closely related to many-body effects including the electron–electron interaction (EEI) and electron–phonon interaction (EPI).

The Kondo effect, which manifests itself in the zero-bias conductance peak or sharp peak of density of states (DOS) at the Fermi energy, was found in bulk metals and semiconductor quantum dots years ago, but has attracted intensive attention again recently in the molecular quantum dot (MQD) [1, 2] due to convenient manipulation. If a tunneling electron travels through a 'soft' MQD, as opposed to a 'hard' semiconductor quantum dot, the molecule can deform from a sphere to a prolate ellipsoid, giving rise to the quantum excitation of internal vibrational (phonon) modes. The current-induced phonon degrees of freedom open inelastic transport channels and give strikingly new physics, such as a series of equally spaced features in differential conductance spectra [3]. The side peaks in the transmission probability or spectral function due to the EPI were found in early theoretical works [4–6]. The phononic effect exists not only in the sequential tunneling but also in the Kondo regime. Recent experiments [7–9] showed that the vibrational sidebands survive in the Kondo regime in nonmagnetic single-molecule transistors, and theoretical efforts [10] were made to understand their origin.

On the other hand, the development in spintronics motivates the study of magnetic tunneling devices where the nonmagnetic lead (N) is replaced with a ferromagnetic lead (F). The F/MQD/F tunnel junction exhibits many novel characteristics. For instance, Kirchner *et al* [11] suggested that a quantum critical point with non-Fermi-liquid behavior can be realized in this magnetic tunnel junction. On the transport aspect, it was argued that the zero-bias Kondo peak may be split due to an exchange magnetic field for parallel (P) alignment of two leads' magnetizations [12–17]. As pointed out by Choi *et al* [17], such an exchange magnetic field arises from the charge fluctuations. Very recently, the theoretical prediction has been verified by the experiment [18]. At the same time, a negative zero-bias tunnel magnetoresistance (TMR) as big as -80% was observed in the Ni/C_{60}–MQD/Ni tunnel junction [18]. Although it can be qualitatively explained by the conductance peak splitting in the P configuration, there has been a quantitative discrepancy between the experiment [18] and theoretical results [12, 19–21] in the zero-bias TMR anomaly. Motivated by the recent experiment [22] where the N/C_{60}–MQD/N junction shows many inelastic characteristics, we have investigated the vibration-mediated transport through an F/MQD/F system and obtained an oscillating TMR with bias voltage due to strong EPI [23]. To the best of our knowledge, there is no other

theoretical study devoted to the vibrating effect on the spin-polarized electron transport through an F/MQD/F junction, although there have been many investigations on nonmagnetic junctions [24–27].

In this paper we focus on the phonon-assisted particle transport through an F/MQD/F junction in the Kondo regime. The phononic effect gives rise to the Franck–Condon factor and modifies relevant parameters (such as the tunneling matrix element), making a great impact on the Kondo effect. A series of phonon-induced Kondo satellites appear in the DOS and tunneling conductance. In the P configuration the Kondo resonance is split and the Kondo satellites deviate from the locations of those in the N/MQD/N junction [10]. The splitting span is narrowed with increasing EPI strength. Another interesting result is that the Kondo peaks in differential conductance undergo a strong suppression in the vicinity of zero bias, leading to the Franck–Condon blockade. In the present work the Franck–Condon blockade appears in the Kondo regime with intermediate coupling, different from what was addressed in the sequential tunneling regime [28], the cotunneling regime [29], and the pair tunneling regime with attractive Coulomb interactions [30]. Finally, the zero-bias TMR ratio is found to be modified by the molecular vibration, depending nonmonotonically upon the EPI strength. The EPI-enhanced negative zero-bias TMR ratio may be about 12% more as compared with that in the absence of EPI, and closer to its experimental value. This paper is organized as follows. In section 2 we present the theoretical model including the EEI and EPI. The Keldysh nonequilibrium Green's function is applied to study the spin-polarized electron transport through an F/MQD/F junction in the Kondo regime. In section 3 we show the variation of Kondo peaks and Kondo satellites with U and EPI strength. In section 4 we calculate differential conductances in the P and antiparallel (AP) configurations. In particular, the Franck–Condon blockade is addressed and a large negative zero-bias TMR is presented. Finally, a brief summary is given in section 5.

2. Theoretical model and method

Consider a single-level molecular quantum dot connected with two F leads, whose magnetic moments are assumed to be collinear (P and AP). Such an F/MQD/F tunnel junction can be described by the Anderson–Holstein model and the model Hamiltonian can be written as $H = \sum_{\alpha\epsilon \mathrm{L,R}} H_\alpha + \hbar\omega_0 a^\dagger a + H_\mathrm{D} + H_\mathrm{T}$. Here $H_\alpha = \sum_{k\sigma} \varepsilon_{k\sigma,\alpha} c^\dagger_{k\sigma,\alpha} c_{k\sigma,\alpha}$ is the Hamiltonian for electrons in the left ($\alpha = \mathrm{L}$) or right ($\alpha = \mathrm{R}$) F leads where $c^\dagger_{k\sigma,\alpha}(c_{k\sigma,\alpha})$ is the creation (annihilation) operator for the electron with wavevector k and spin σ in lead α, and $\varepsilon_{k\sigma,\alpha}$ is the spin-dependent single-electron energy. In the phonon Hamiltonian $a^\dagger(a)$ creates (annihilates) a phonon with frequency ω_0. With the EEI and EPI included, the molecular dot Hamiltonian reads

$$H_\mathrm{D} = \sum_\sigma [\varepsilon_\sigma + \lambda(a^\dagger + a)] n_\sigma + U n_\uparrow n_\downarrow, \tag{1}$$

where $n_\sigma = d^\dagger_\sigma d_\sigma$ is the number operator of the spin-σ electron on the MQD with single-level ε_σ, λ is the EPI coupling strength, and U is the on-site Coulomb repulsion parameter. The average of n_σ can be controlled by modulating the gate voltage. The traveling electron can hop between the molecule dot and leads, which can be described by the tunneling Hamiltonian, $H_\mathrm{T} = \sum_{k\sigma,\alpha\in \mathrm{L,R}} T_{k\sigma,\alpha} c^\dagger_{k\sigma,\alpha} d_\sigma + \mathrm{H.c.}$, with $T_{k\sigma,\alpha}$ the spin-dependent tunneling matrix element.

Following Meir and Wingreen [31], by use of the Keldysh nonequilibrium Green function formalism, the current through the system turns out to be

$$I_\sigma = \frac{-e^2}{2\pi\hbar} \int \mathrm{d}\omega\, [f_\mathrm{L}(\omega) - f_\mathrm{R}(\omega)] \frac{\Gamma_{\mathrm{L},\sigma}\Gamma_{\mathrm{R},\sigma}}{\Gamma_{\mathrm{R},\sigma} + \Gamma_{\mathrm{L},\sigma}} \mathrm{Im}\, G^\mathrm{r}_\sigma(\omega), \tag{2}$$

where $G^\mathrm{r}(\omega)$ is the retarded Green's function for the dot electron in which the correlations due to both EEI and EPI, together with coupling to the leads, are included. $\Gamma_{\alpha,\sigma} = 2\pi\rho_{\alpha,\sigma}\sum_k |T_{k\sigma,\alpha}|^2$ is the level-width function with $\rho_{\alpha,\sigma}$ the spin-dependent DOS at the Fermi level in lead α. $f_\mathrm{L}(\omega)$ and $f_\mathrm{R}(\omega)$ are the Fermi distribution functions of the left and right leads, respectively, in which the chemical potentials measured with respect to the Fermi energy at $V_\mathrm{bias} = 0$ are given by $\mu_\mathrm{L} = -\mu_\mathrm{R} = eV_\mathrm{bias}/2$ with V_bias the bias voltage applied to the junction.

Performing a canonical transformation, $\tilde{H} = \mathrm{e}^s H \mathrm{e}^{-s} = \tilde{H}_\mathrm{el} + \hbar\omega_0 a^\dagger a$, with $s = \lambda/\omega_0 \sum_\sigma n_\sigma (a^\dagger - a)$, to decouple the entanglement of electron and phonon, we obtain

$$\tilde{H}_\mathrm{el} = \sum_{k\sigma,\alpha\in \mathrm{L,R}} \varepsilon_{k\sigma,\alpha} c^\dagger_{k\sigma,\alpha} c_{k\sigma,\alpha} + \sum_\sigma \tilde{\varepsilon}_\sigma n_\sigma + \tilde{U} n_\uparrow n_\downarrow + \sum_{k\sigma,\alpha\in \mathrm{L,R}} (\tilde{T}_{k\sigma,\alpha} c^\dagger_{k\sigma,\alpha} d_\sigma + \mathrm{H.c.}). \tag{3}$$

This transformation renormalizes relevant parameters as $\tilde{\varepsilon}_\sigma = \varepsilon_\sigma - \Delta$ and $\tilde{U} = U - 2\Delta$ where $\Delta = g\omega_0$ with $g = (\lambda/\omega_0)^2$, and $\tilde{T}_{k\sigma,\alpha} = T_{k\sigma,\alpha} X$ with $X = \exp[-\lambda/\omega_0 (a^\dagger - a)]$. The renormalized tunneling matrix element $\tilde{T}_{k\sigma,\alpha}$ contains the phonon operator, indicating that the electron hopping processes between the dot and leads have been subject to modification of inelastic scattering, in which new phonon tunneling channels develop accompanied by polaron formation. The renormalized electron (i.e. polaron) Hamiltonian $\tilde{H}_\mathrm{el}$, which includes the joint effect of EEI and EPI, becomes a typical Anderson model if $\tilde{T}_{k\sigma,\alpha}$ is approximately replaced by its expectation value $\tilde{T}_{k\sigma,\alpha} = T_{k\sigma,\alpha}\langle X\rangle = T_{k\sigma,\alpha}\mathrm{e}^{-g(N_\mathrm{ph}+1/2)}$ with $N_\mathrm{ph} = 1/[\exp(\omega_0/k_\mathrm{B}T) - 1]$ the phonon number. This approximation is reasonable provided the relaxation time of phonons is much shorter than the time of the electron transport through the dot so that the phonon subsystem remains in thermal equilibrium. The same approximation has been adopted by other works [10, 23, 32, 33]. In the polaron representation the original MQD Green's function can be written as

$$G^\mathrm{r}(t) = \tilde{G}^\mathrm{r}(t)\langle X(t)X^\dagger\rangle_\mathrm{ph} + \theta(t)\tilde{G}^<(t)(\langle X(t)X^\dagger\rangle_\mathrm{ph} - \langle X^\dagger X(t)\rangle_\mathrm{ph}), \tag{4}$$

where $\tilde{G}^\mathrm{r}(t) = -\mathrm{i}\theta(t)\langle[\tilde{d}_\sigma(t), d^\dagger_\sigma]_+\rangle_\mathrm{el}$ and $\tilde{G}^<(t) = \mathrm{i}\langle d^\dagger_\sigma \tilde{d}_\sigma(t)\rangle_\mathrm{el}$ with $\tilde{d}_\sigma(t) = \mathrm{e}^{\mathrm{i}\tilde{H}_\mathrm{el}t} d_\sigma \mathrm{e}^{-\mathrm{i}\tilde{H}_\mathrm{el}t}$ are the retarded and lesser Green's functions associated with Hamiltonian (3), and $X(t) = \mathrm{e}^{\mathrm{i}\tilde{H}_\mathrm{ph}t} X \mathrm{e}^{-\mathrm{i}\tilde{H}_\mathrm{ph}t}$. The Franck–Condon factors

are given by $\langle X(t)X^{\dagger}\rangle_{\rm ph} = \exp[-\Phi(t)]$ and $\langle X^{\dagger}X(t)\rangle_{\rm ph} = \exp[-\Phi(-t)]$, respectively associated with electron and hole transport, with $\Phi(t) = g[N_{\rm ph}(1-{\rm e}^{{\rm i}\omega_0 t}) + (N_{\rm ph}+1)(1-{\rm e}^{-{\rm i}\omega_0 t})]$ [33]. As has been discussed previously [23, 32], $\exp[-\Phi(t)]$ and $\exp[-\Phi(-t)]$ are generally different from each other. The Fourier transformation of $G^{\rm r}(t)$ in equation (4) can be easily obtained as

$$G^{\rm r}_{\sigma}(\omega) = \sum_{n=-\infty}^{\infty} L_n\{[1-\bar{f}_{\sigma}(\omega-n\omega_0)]\tilde{G}^{\rm r}_{\sigma}(\omega-n\omega_0) + \bar{f}_{\sigma}(\omega+n\omega_0)\tilde{G}^{\rm r}_{\sigma}(\omega+n\omega_0)\}, \tag{5}$$

where

$$\bar{f}_{\sigma}(\omega) = [\Gamma_{{\rm L},\sigma} f_{\rm L}(\omega) + \Gamma_{{\rm R},\sigma} f_{\rm R}(\omega)]/(\Gamma_{{\rm L},\sigma}+\Gamma_{{\rm R},\sigma}), \tag{6}$$

and $L_n = {\rm e}^{-g(2N_{\rm ph}+1)}{\rm e}^{n\omega_0/2k_{\rm B}T} I_n[2g\sqrt{N_{\rm ph}(N_{\rm ph}+1)}]$ with $I_n(x)$ as the modified nth Bessel function. By use of the equation of motion (EOM) approach [34], the retarded Green function $\tilde{G}^{\rm r}_{\sigma}(\omega)$ in equation (5) is obtained as

$$\tilde{G}^{\rm r}_{\sigma}(\omega) = \frac{1-\langle n_{\bar\sigma}\rangle}{\omega-\tilde{\varepsilon}_{\sigma}-\tilde{\Sigma}^{\rm r}_{0\sigma}+\tilde{U}\tilde{\Sigma}^{\rm r}_{1\sigma}(\omega-\tilde{\varepsilon}_{\sigma}-\tilde{U}-\tilde{\Sigma}^{\rm r}_{0\sigma}-\tilde{\Sigma}^{\rm r}_{3\sigma})^{-1}} + \frac{\langle n_{\bar\sigma}\rangle}{\omega-\tilde{\varepsilon}_{\sigma}-\tilde{U}-\tilde{\Sigma}^{\rm r}_{0\sigma}-\tilde{U}\tilde{\Sigma}^{\rm r}_{2\sigma}(\omega-\tilde{\varepsilon}_{\sigma}-\tilde{\Sigma}^{\rm r}_{0\sigma}-\tilde{\Sigma}^{\rm r}_{3\sigma})^{-1}}, \tag{7}$$

where the retarded self-energies due to coupling between the dot and leads and due to the EEI are given by

$$\begin{aligned}
\tilde{\Sigma}^{\rm r}_{0\sigma}(\omega) &= \sum_{\alpha\epsilon{\rm L,R}}\int\frac{{\rm d}\varepsilon}{2\pi}\frac{\tilde{\Gamma}_{\alpha,\sigma}}{\omega-\varepsilon},\\
\tilde{\Sigma}^{\rm r}_{3\sigma}(\omega) &= \sum_{\alpha\epsilon{\rm L,R}}\int\frac{{\rm d}\varepsilon}{2\pi}\tilde{\Gamma}_{\alpha,\bar\sigma}\left(\frac{1}{\omega-\varepsilon-\tilde{\varepsilon}_{\sigma}+\tilde{\varepsilon}_{\bar\sigma}}+\frac{1}{\omega+\varepsilon-\tilde{\varepsilon}_{\sigma}-\tilde{\varepsilon}_{\bar\sigma}-\tilde{U}}\right),\\
\tilde{\Sigma}^{\rm r}_{1\sigma}(\omega) &= \sum_{\alpha\epsilon{\rm L,R}}\int\frac{{\rm d}\varepsilon}{2\pi}\tilde{\Gamma}_{\alpha,\bar\sigma}f_{\alpha}(\varepsilon)\left(\frac{1}{\omega-\varepsilon-\tilde{\varepsilon}_{\sigma}+\tilde{\varepsilon}_{\bar\sigma}}+\frac{1}{\omega+\varepsilon-\tilde{\varepsilon}_{\sigma}-\tilde{\varepsilon}_{\bar\sigma}-\tilde{U}}\right)\\
\tilde{\Sigma}^{\rm r}_{2\sigma}(\omega) &= \tilde{\Sigma}^{\rm r}_{1\sigma}(\omega)-\tilde{\Sigma}^{\rm r}_{3\sigma}(\omega),
\end{aligned} \tag{8}$$

with $\tilde{\Gamma}_{\alpha,\sigma} = {\rm e}^{-g(2N_{\rm ph}+1)}\Gamma_{\alpha,\sigma}$. The averaged occupation number $\langle n_{\sigma}\rangle$ of the particle on the MQD is given by

$$\langle n_{\sigma}\rangle = -\int\frac{{\rm d}\omega}{\pi}\bar{f}_{\sigma}(\omega)\,{\rm Im}\,G^{\rm r}_{\sigma}(\omega), \tag{9}$$

which can be evaluated self-consistently by equations (5)–(9) with spin $\bar\sigma$ opposite to σ.

In the Kondo regime in which both charge and spin fluctuations play an important role, the dot bare level $\tilde{\varepsilon}_{\sigma}$ should be renormalized to $\breve{\varepsilon}_{\sigma}$ [12, 13, 19, 20, 35]. As a result of the renormalization, the original degenerate dot levels are split, equivalent to the contribution of an effective exchange magnetic field $gu_{\rm B}B^{(\pm n)}_{\rm eff} = \breve{\varepsilon}^{(\pm n)}_{\downarrow} - \breve{\varepsilon}^{(\pm n)}_{\uparrow}$, namely

$$gu_{\rm B}B^{(\pm n)}_{\rm eff} = -\,{\rm Re}\sum_{\alpha\epsilon{\rm L,R}}\int\frac{{\rm d}\varepsilon}{2\pi}f_{\alpha}(\varepsilon)\times\left[\tilde{\Gamma}_{\alpha,\uparrow}\left(\frac{1}{\varepsilon\pm n\omega_0-\breve{\varepsilon}^{(\pm n)}_{\uparrow}}+\frac{1}{-\varepsilon\pm n\omega_0+\tilde{U}+\breve{\varepsilon}^{(\pm n)}_{\uparrow}}\right) - \tilde{\Gamma}_{\alpha,\downarrow}\left(\frac{1}{\varepsilon\pm n\omega_0-\breve{\varepsilon}^{(\pm n)}_{\downarrow}}+\frac{1}{-\varepsilon\pm n\omega_0+\tilde{U}+\breve{\varepsilon}^{(\pm n)}_{\downarrow}}\right)\right] \tag{10}$$

which is appropriate for the finite U case [19, 20, 35]. In the present work this self-consistent procedure is applied not only to the phonon number $n = 0$ case but also to finite n cases. The latter comes from the self-energy $\tilde{\Sigma}^{\rm r}_{1\sigma}(\omega\pm n\omega_0)$ included in $\tilde{G}^{\rm r}_{\sigma}(\omega\pm n\omega_0)$ of equation (5), where $+n$ $(-n)$ corresponds to the electron (hole) transport accompanied by n-phonon emission. The level splitting in the P alignment can be regarded as a result of the effective exchange magnetic field coming from the two F leads with parallel magnetization.

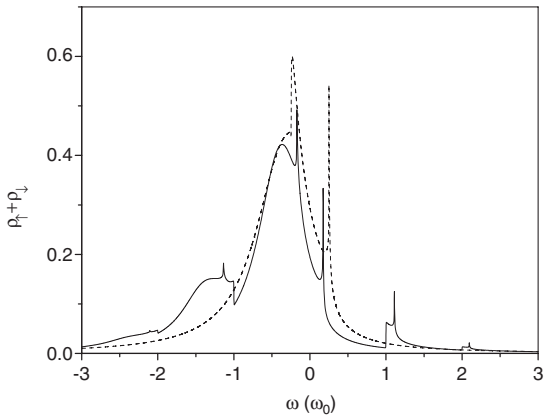

Figure 1. Density of states $\rho_{\uparrow}+\rho_{\downarrow}$ as a function of energy ω in parallel alignment of magnetization in the absence of EPI (dashed line) and in the presence of EPI with $\lambda = 0.5$ (solid line). The other parameters are $U = 50$.

3. Density of states

In what follows we present some numerical results for Kondo resonances. The spin polarization of the two F leads the same is defined as $P = (\rho_{\uparrow}-\rho_{\downarrow})/(\rho_{\uparrow}+\rho_{\downarrow})$ with $\rho_{\uparrow}$ $(\rho_{\downarrow})$ the electronic DOS for the majority (minority) spin subbands. The renormalized level-width functions are given by $\tilde{\Gamma}_{{\rm L}\sigma} = {\rm e}^{-g(2N_{\rm ph}+1)}\Gamma_{\rm L0}(1+\sigma_z P)$ and $\tilde{\Gamma}_{{\rm R}\sigma} = {\rm e}^{-g(2N_{\rm ph}+1)}\Gamma_{\rm R0}(1\pm\sigma_z P)$ where the sign $\pm$ stands for the P or AP magnetization alignment of the two F leads. Several parameters are taken in the numerical calculations: $P = 0.31$, $\Gamma_{\rm L0} = \Gamma_{\rm R0} = 0.2$, and $\tilde{\varepsilon}_{\uparrow} = \tilde{\varepsilon}_{\downarrow} = \tilde{\varepsilon}_0 = -0.45$ with phonon frequency ω_0 as the energy unit. The temperature is given by $T/T_{\rm K} = 0.05$, with $T_{\rm K}$ the Kondo temperature at $\lambda = 0$ [17].

The spin-resolved DOS can be obtained as $\rho_{\sigma}(\varepsilon) = -(1/\pi)\,{\rm Im}\,G^{\rm r}_{\sigma}(\varepsilon)$, in which the expression for $G^{\rm r}_{\sigma}(\varepsilon)$ is given by equation (5). In figure 1 we plot the total DOS, $\rho_{\uparrow}+\rho_{\downarrow}$, as

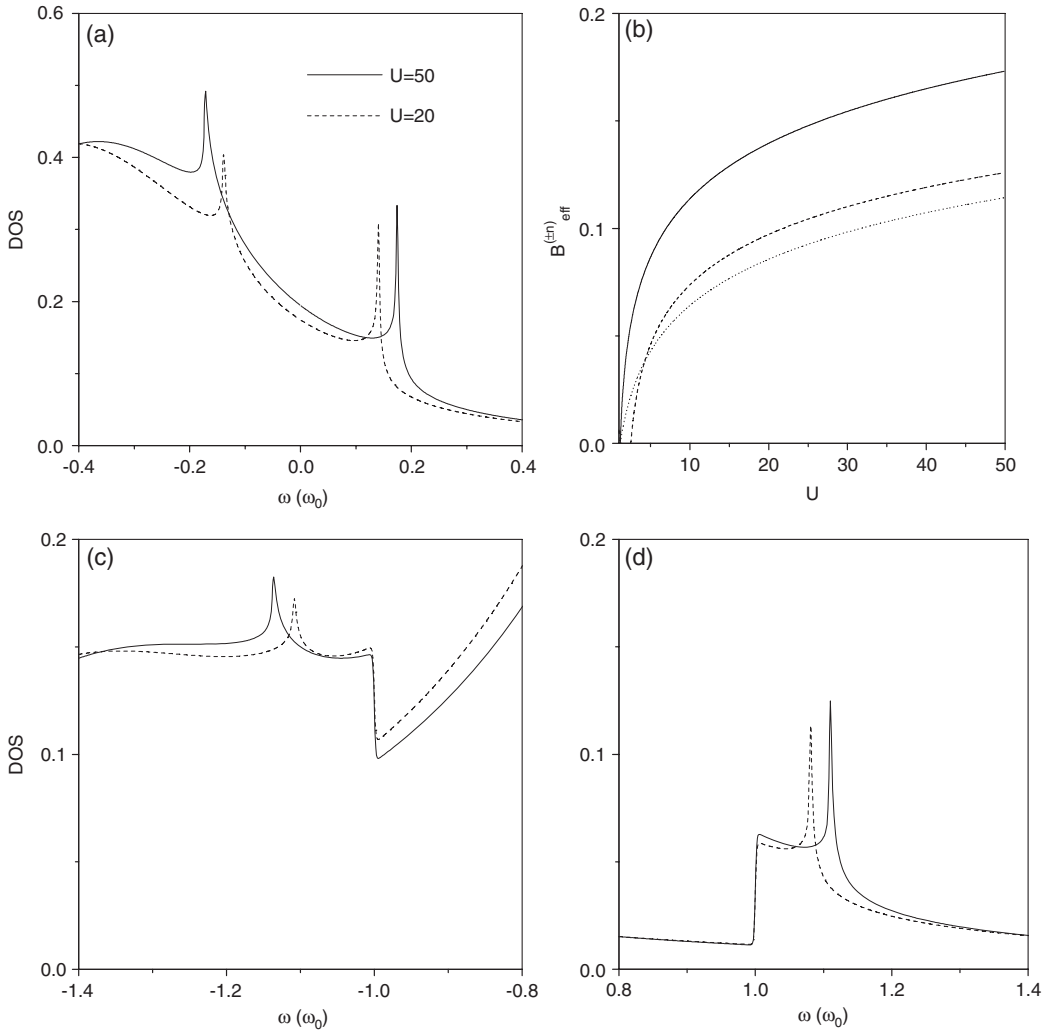

Figure 2. Density of states for Kondo resonances (a), and phonon-assisted Kondo satellites for hole (c) and electron (d) with $U = 20$ (dashed line) and $U = 50$ (solid line) in parallel alignment of magnetization. The effective exchange fields $B_{\rm eff}^{(0)}$ (solid line), $B_{\rm eff}^{(-1)}$ (dashed line), and $B_{\rm eff}^{(+1)}$ (dotted line) as a function of U are given in (b). The other parameters are $\lambda = 0.5$.

a function of incident electron energy ω in the P magnetization configuration for $V_{\rm bias} = 0$. In the absence of EPI, in addition to an elastic resonant peak at $\omega = \tilde{\varepsilon_0} = -0.45$, there appear two sharp Kondo resonance peaks separately located on both sides of Fermi energy $E_{\rm F} = 0$, as shown by the dashed line in figure 1. Unlike in an N/MQD/N junction, in which the single Kondo peak is exactly located at $E_{\rm F}$, the double Kondo peaks in the F/MQD/F junction are at $\pm(\breve{\varepsilon}_{\uparrow}^{(0)} - \breve{\varepsilon}_{\downarrow}^{(0)})$, exhibiting a large splitting $2B_{\rm eff}^{(0)}$ with $gu_{\rm B} = 1$ taken. When inelastic phonon channels are turned on, shown from the solid line in figure 1, a series of smaller phonon-assisted Kondo satellites appear on both sides of the Kondo peaks. Their positions are $\omega = \pm(n\omega_0 + B_{\rm eff}^{(\pm n)})$, deviating from $\omega = \pm n\omega_0$ where there are sharp lineshapes due to the Fermi distribution function, which becomes a unit-step function at low temperatures [10, 32]. It is worth mentioning that the positions of phonon-assisted Kondo satellites are exactly at $\omega = \pm n\omega_0$ in N/MQD/N junctions [10].

In figure 2 we plot the blowups of the DOS for the Kondo peaks (a) and Kondo satellites (c) and (d). As indicated from figures 2(c) and (d), there are two types of Kondo satellites: the holelike Kondo satellite at $-\omega_0 - B_{\rm eff}^{(-1)}$ and the electron-like Kondo satellite at $\omega_0 + B_{\rm eff}^{(+1)}$. Both of them arise from the phonon emission in the process of spin exchange for the hole and electron tunneling through the MQD from one lead to the other, as will be discussed below. One can further find that either of the shifts $B_{\rm eff}^{(-1)}$ for the holelike Kondo satellite in figure 2(c) and $B_{\rm eff}^{(+1)}$ for the electron-like Kondo satellite in figure 2(d) is smaller than $B_{\rm eff}^{(0)}$ for the Kondo peak in figure 2(a), and that $B_{\rm eff}^{(-1)}$ is not equal to $B_{\rm eff}^{(+1)}$ due to asymmetry of the electron and hole in the system under consideration. The U dependence of $B_{\rm eff}^{(0)}$, $B_{\rm eff}^{(-1)}$, and $B_{\rm eff}^{(+1)}$ is presented in figure 2(b). A comparison between solid and dashed lines in figures 2(a), (c) and (d) indicates that, with the correlation parameter U enhanced, the splitting becomes larger and the Kondo peaks become higher.

Figure 3(a) shows the variation of the Kondo resonances with the EPI coupling parameter λ. It is found that with increasing λ the splitting span of the double Kondo peaks

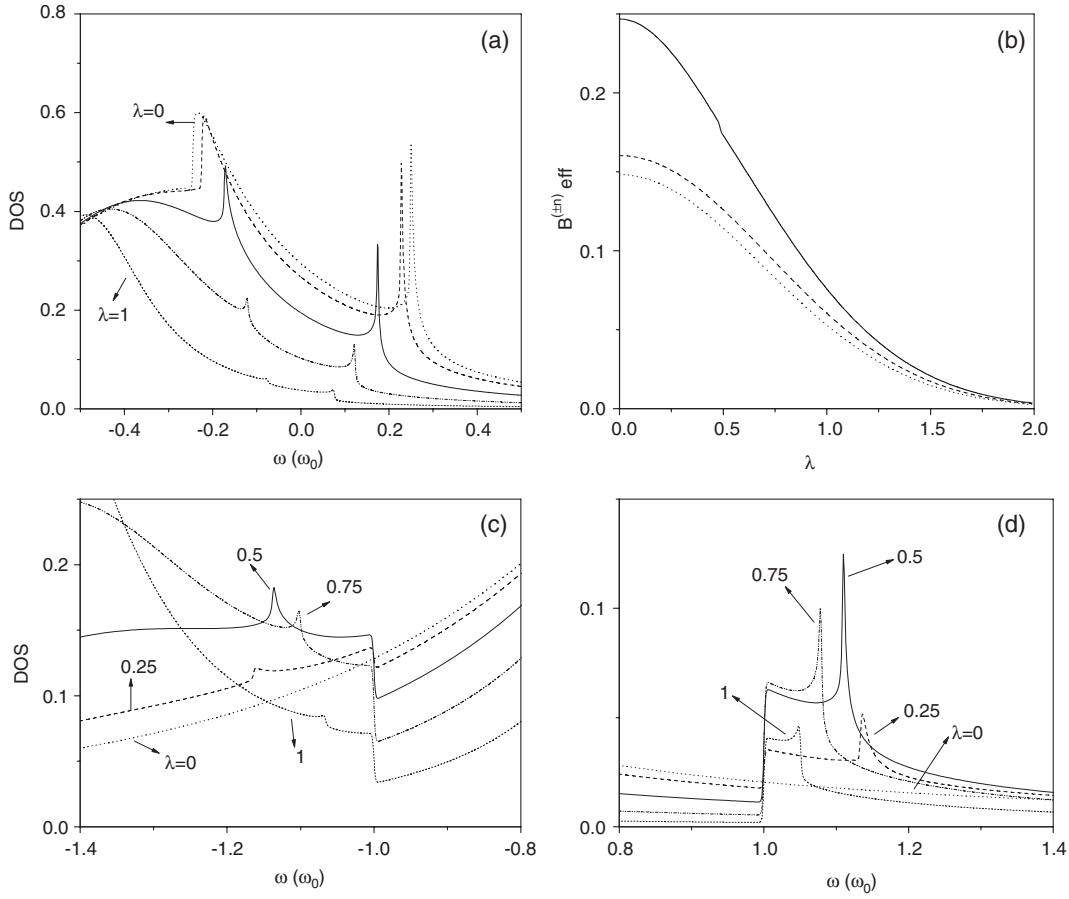

Figure 3. Density of states for Kondo resonances with λ increased from top to bottom in (a) and phonon-assisted Kondo satellites with λ as indicated in (c) and (d). The effective exchange fields $B_{\rm eff}^{(0)}$ (solid line), $B_{\rm eff}^{(-1)}$ (dashed line), and $B_{\rm eff}^{(+1)}$ (dotted line) as a function of λ are given in (b). The magnetization is in the parallel alignment and the other parameters are the same as in figure 1.

becomes small due to the parameter renormalization by the phononic effect. In addition to $B_{\rm eff}^{(0)}$, either $B_{\rm eff}^{(-1)}$ or $B_{\rm eff}^{(+1)}$ is a monotonically decreasing function of λ, as shown in figure 3(b). At the same time, both Kondo peaks and their background are monotonically lower with λ increased. When λ is large enough, there appears a strong suppression of DOS, which will have a great impact on transport properties, which will be seen in figures 5 and 6. In figures 3(c) and (d), there is no Kondo satellite at $\lambda = 0$ because it is of EPI origin. Another characteristic of figures 3(c) and (d) is the nonmonotonic dependence of the magnitude of the Kondo satellite on λ. It first increases with λ and then decreases, exhibiting a maximum at a certain value of λ. This nonmonotonic behavior is attributable to two types of competing mechanisms. One is that a stronger EPI can enhance the phonon emission through which the phonon-assisted Kondo spin singlet forms, favorable to formation of Kondo satellites. The other is that an increasing λ can reduce the effective coupling between the dot and leads, i.e., $\tilde{\Gamma}_{\alpha,\sigma} = {\rm e}^{-g(2N_{\rm ph}+1)}\Gamma_{\alpha,\sigma}$ with $g \propto \lambda^2$, which is unfavorable for the Kondo satellite.

The discussion above is suitable only for the P magnetization configuration. In the AP configuration the situation is quite different, in which there is neither splitting of the Kondo peak nor $B_{\rm eff}^{(\pm n)}$ for $\Gamma_{\rm L0} = \Gamma_{\rm R0}$. Since the exchange fields arising from the left and right leads have opposite directions and cancel each other out, the Kondo effect in the symmetric F/MQD/F junction with the AP configuration is similar to that in the N/MQD/N junctions. The further calculations show that if $\Gamma_{\rm L0} \neq \Gamma_{\rm R0}$ the spin splitting appears even in the AP alignment. In order to capture the physics of phonon effects, here we focus attention on the symmetric case of $\Gamma_{\rm L0} = \Gamma_{\rm R0}$.

4. Differential conductance and tunneling magnetoresistance

We now study nonequilibrium transport properties of the F/MQD/F junction subject to a bias voltage. Figure 4 gives a schematic depiction of spin-polarized electron tunneling through the MQD. In the P configuration, there are two split levels on the MQD: $\breve{\varepsilon}_{\uparrow}^{(+n)} = \tilde{\varepsilon_0} - \frac{1}{2}B_{\rm eff}^{(+n)}$ and $\breve{\varepsilon}_{\downarrow}^{(+n)} = \tilde{\varepsilon_0} + \frac{1}{2}B_{\rm eff}^{(+n)}$, e.g. with $n = 1$ in figure 4(a) and $n = 0$ in figure 4(b). As a spin-down electron on the Fermi surface tunnels from the left lead onto the dot, it will inhabit the upper level $\breve{\varepsilon}_{\downarrow}^{(+n)}$; at the same time, a spin-up electron on the lower level $\breve{\varepsilon}_{\uparrow}^{(+n)}$ tunnels out to the right lead. The Kondo resonance is a consequence of formation of a Kondo spin singlet, i.e. a kind of high-order process with spin exchange. In the absence of EPI, the elastic

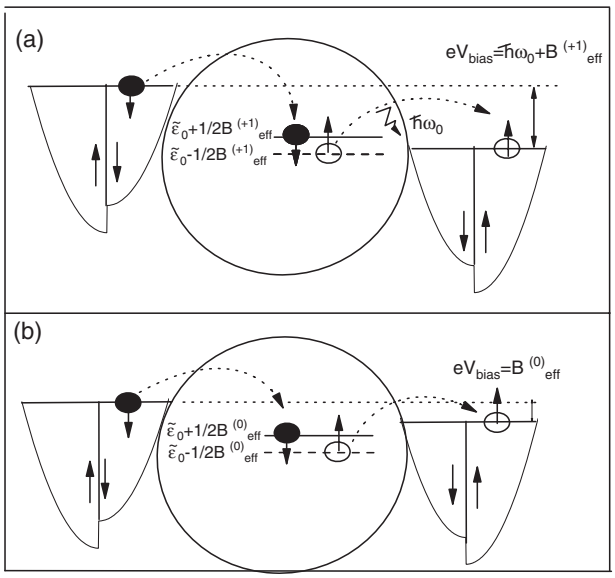

Figure 4. Schematic diagram for formation of the Kondo spin singlet for the $n = 1$ Kondo satellite with an electron emitting one phonon (a) and the Kondo peak (b).

Kondo tunneling process is shown in figure 4(b), in which the Kondo resonance appears for applied bias $eV_{\rm bias}$ equal to spin-exchange energy $B_{\rm eff}^{(0)} = \breve{\varepsilon}_{\downarrow}^{(0)} - \breve{\varepsilon}_{\uparrow}^{(0)}$. Participation of phonons makes matters somewhat complicated. Figure 4(a) shows the inelastic process leading to Kondo resonance formation, in which a phonon of ω_0 is emitted. In this case, there will appear a phonon-related Kondo satellite at bias $B_{\rm eff}^{(+n)} + n\omega_0$ with $n = 1$. At low temperatures under consideration, only phonon emission is relevant because there is no available phonon in the MQD, which has been confirmed in our calculations. Similar to the electron tunneling processes in figure 4, there are elastic and inelastic resonance tunnelings for holes, the corresponding biases equal to $-B_{\rm eff}^{(0)}$ and $-B_{\rm eff}^{(-n)} - n\omega_0$, respectively.

In figure 5 the differential conductance defined as $G_\sigma = \partial I_\sigma / \partial V_{\rm bias}$ is plotted as a function of bias $V_{\rm bias}$ for the P (a) and AP (b) configurations. An important distinction between them is that, while in the AP alignment there is a zero-bias conductance peak (ZBCP), in the P alignment it splits due to appearance of $B_{\rm eff}^{(0)}$ so that a zero-bias conductance dip (ZBCD) forms. As the bias increases up to values of $eV_{\rm bias} = \pm B_{\rm eff}^{(0)}$, there appear sharp conductance resonances, corresponding to the process in figure 4(b). Such a difference between ZBCD and ZBCP behavior for the P and AP configurations, respectively, may lead to a negative zero-bias TMR ratio, which is defined as TMR $= (G_{\rm P} - G_{\rm AP})/G_{\rm AP}$. The electron–phonon coupling is taken to be $\lambda = 0$, 0.25, 0.5, 0.75, and 1 for curves from top to bottom in figure 5. It is found from figure 5(a) that with increasing λ the splitting distance between the Kondo sub-peaks of $G_{\rm P}$ decreases. Another difference between $G_{\rm P}$ and $G_{\rm AP}$ is that smaller peaks of $G_{\rm P}$ appear at $eV_{\rm bias} = \pm(B_{\rm eff}^{(\pm 1)} + \omega_0)$, which are the combinative contribution from the phonon resonance and Kondo phonon satellites, corresponding to the process shown in figure 4(a).

On the other hand, it is seen from figure 5 that with increasing λ the differential conductance quickly decreases and eventually is closely vanishing in the vicinity of zero bias. This conduction suppression behavior for larger λ continues until there appear phonon-assisted resonant tunneling processes. From current $I_{\rm P}$ versus bias curves, whose slope corresponds to the differential conductance, shown in the inset of figure 5(a), it can be seen that with increasing λ the slope of the V–I curve gradually becomes flat in the bias range from $-\omega_0$ to ω_0, which is the origin of conductance suppression. The same current suppression also occurs for the AP alignment. Such a current suppression arises from the change of L_n in equation (5), which is closely related to the Frank–Condon factor $\Phi(t)$. L_n decreases exponentially with λ^2, leading to the Franck–Condon blockade for larger λ. The physics underlying is that a stronger EPI leads to more overlap between the electron and phonon wavefunctions. The formation of polaron can trap the transport particle and is unfavorable for conductance at low bias. This case can be released until the bias voltage is high enough to give rise to resonance (i.e. the process of emission of a phonon). Phonon-assisted tunneling appears if $eV_{\rm bias}$ gets to the vicinity of $\pm n\omega_0$. This Franck–Condon blockade has been suggested recently in the regimes of the sequential tunneling [28], the cotunneling [29], and the pair tunneling with strong EPI [30]. In the present work this concept is applied to the Kondo regime with intermediate EPI coupling.

Figure 6(a) shows the TMR ratio as a function of bias voltage, exhibiting a change from negative to positive with increasing $V_{\rm bias}$. Negative zero-bias TMR ratios are obtained, which may be used to explain the experimental data [18]. It is found that with increasing λ the zero-bias TMR exhibits a nonmonotonic change, having the maximal value of about -62% at $\lambda = 0.5$. This nonmonotonic dependence can be also seen by the solid line of figure 6(b), in which the variation of the TMR ratio is plotted as a function of λ. As shown by the dashed lines in figure 6(b), at zero bias, $G_{\rm AP}$ is always greater than $G_{\rm P}$, both of them decreasing with λ increasing. Since $G_{\rm AP}$ decreases faster than $G_{\rm P}$, the zero-bias TMR ratio (or $G_{\rm P}/G_{\rm AP}$) exhibits a nonmonotonic change with λ. The fact that $G_{\rm AP}$ is always greater than $G_{\rm P}$ at zero bias is closely associated with the formation of the Kondo spin singlet in the tunneling process, as shown in figure 4(b); and their λ dependence arises from the EPI-induced renormalization of parameters; e.g., $L_n(\lambda^2)$ in equation (5) decreases exponentially with λ^2. Compared with the TMR ratio in the absence of EPI, the electron–phonon coupling makes the negative TMR ratio greater (its maximum reaches about -62%). This result is in between the experimental data (-80%) [18] and theoretical result (about -50%) in the absence of EPI [12, 19, 21, 36].

5. Summary

In summary we have analyzed the Kondo effect in electron transport through a single-molecule quantum dot coupled to two F leads by applying the nonequilibrium Green's function approach and by taking into account the EEI with finite U and EPI. In the P configuration, the Kondo peak in the DOS is split, and a series of new phonon-induced Kondo satellites develops on both sides of the Fermi energy. The positions

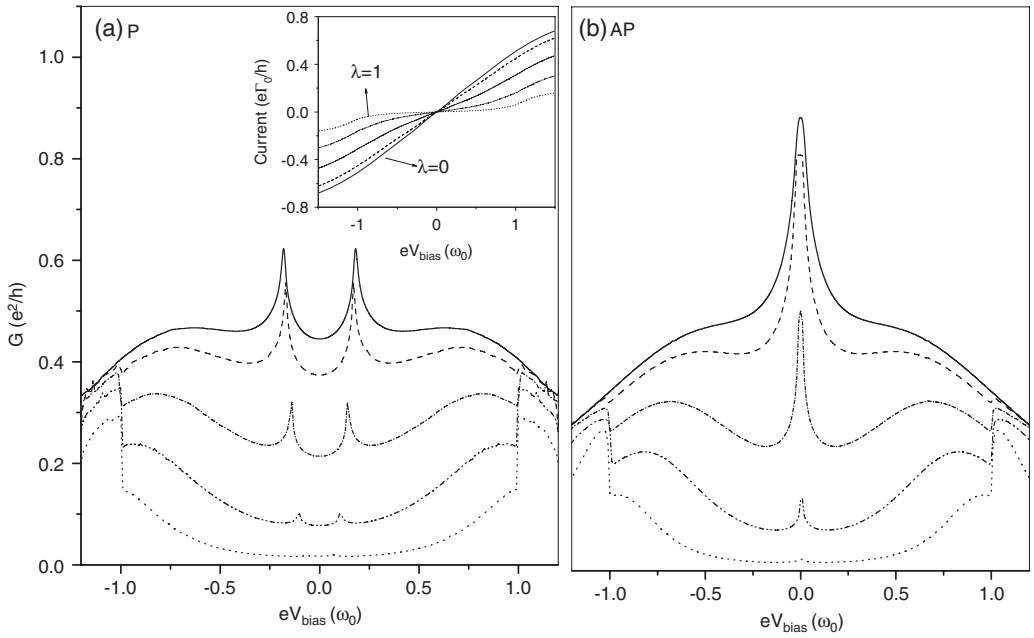

Figure 5. Differential conductance as a function of bias voltage for $\lambda = 0$, 0.25, 0.5, 0.75, and 1 from top to bottom in the parallel (a) and antiparallel (b) configurations. In the inset there are I–V curves corresponding to (a). The other parameters are the same as in figure 1.

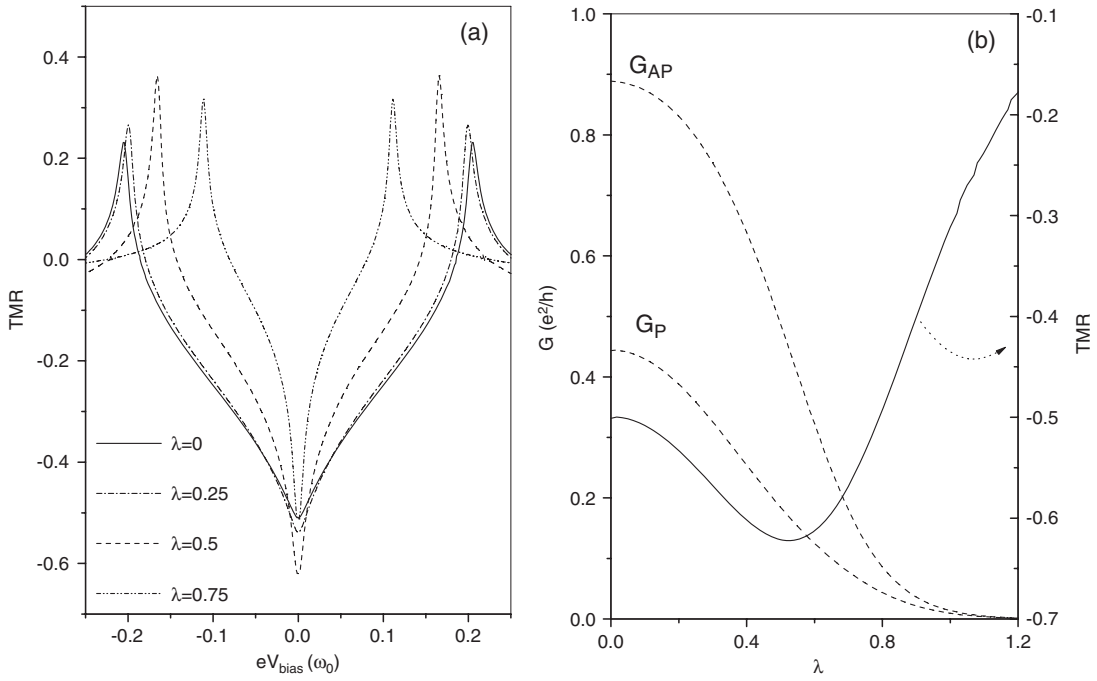

Figure 6. (a) TMR ratios as a function of bias voltage with $\lambda = 0$, 0.25, 0.5, and 0.75 and (b) TMR ratio (solid line), G_{P}, and G_{AP} (dashed lines) as functions of λ at zero bias. The other parameters are the same as in figure 1.

of the Kondo satellites in the DOS deviates from those in the N/MQD/N junction, for an effective exchange field is induced on the dot by two F leads with parallel magnetizations. The splitting of the Kondo peak and the Kondo satellites (electron-like and holelike) are dependent upon both U and λ. Another interesting result is the Franck–Condon blockade in the Kondo regime, where the current in the vicinity of zero bias is strongly quenched by strong electron–phonon coupling. Finally, a big negative zero-bias TMR ratio is presented, which arises from the ZBCP behavior in the AP configuration and ZBCD behavior in the P configuration. It is shown that the negative zero-bias TMR effect depends nonmonotonically upon the EPI strength. For an appropriate EPI, the zero-bias TMR can be enhanced to reach -62%, which is greater than the -50% obtained previously in the absence of EPI and closer to its experimental value of -80%.

Acknowledgments

This work is supported by the National Natural Science Foundation of China under grant No 90403011, and also by the State Key Program for Basic Research of China under grant Nos 2006CB921803 and 2004CB619004.

References

[1] Liang W, Shores M P, Bockrath M, Long J R and Park H 2002 *Nature* **417** 725
[2] Park J, Pasupathy A N, Goldsmith J I, Chang C, Yaish Y, Petta J R, Rinkowski M, Sethna J P, Abruña H D, McEuen P L and Ralph D C 2002 *Nature* **417** 722
[3] Qiu X H, Nazin G V and Ho W 2004 *Phys. Rev. Lett.* **92** 206102
[4] Wingreen N S, Jacobsen K W and Wilkins J W 1988 *Phys. Rev. Lett.* **61** 1396
[5] Glazman L I and Shekhter R I 1987 *Zh. Eksp. Teor. Fiz.* **94** 292 Glazman L I and Shekhter R I 1988 *Sov. Phys.—JETP* **67** 163 (Engl. Transl.)
[6] Jonson M 1989 *Phys. Rev.* B **39** 5924
[7] Yu L H, Keane Z K, Ciszek J W, Cheng L, Stewart M P, Tour J M and Natelson D 2004 *Phys. Rev. Lett.* **93** 266802
[8] Yu L H and Natelson D 2004 *Nano Lett.* **4** 79
[9] Yu L H and Natelson D 2004 *Nanotechnology* **15** S517
[10] Chen Z Z, Lu H Z, Lü R and Zhu B F 2006 *J. Phys.: Condens. Matter* **18** 5435
[11] Kirchner S, Zhu L J, Si Q M and Natelson D 2005 *Proc. Natl Acad. Sci. USA* **102** 18824
[12] Martinek J, Utsumi Y, Imamura J, Barnaś J, Maekawa S, König J and Schön G 2003 *Phys. Rev. Lett.* **91** 127203
[13] Zhang P, Xue Q K, Wang Y P and Xie X C 2002 *Phys. Rev. Lett.* **89** 286803
[14] Dong B, Cui H L, Liu S Y and Lei X L 2003 *J. Phys.: Condens. Matter* **15** 8435
[15] López R and Sánchez D 2003 *Phys. Rev. Lett.* **90** 116602
[16] Sergueev N, Sun Q F, Guo H, Wang B G and Wang J 2002 *Phys. Rev.* B **65** 165303
[17] Choi M S, Sánchez D and López R 2004 *Phys. Rev. Lett.* **92** 056601
[18] Pasupathy A N, Bialczak R C, Martinek J, Grose J E, Donev L A K, Mceuen P L and Ralph D C 2004 *Science* **86** 306
[19] Świrkowicz R, Wilczyński M and Barnaś J 2006 *J. Phys: Condens. Matter* **18** 2291
[20] Martinek J, Sindel M, Borda L, Barnaś J, Bulla R, König J, Schön G, Maekawa S and von Delft J 2005 *Phys. Rev.* B **72** 121302(R)
[21] Świrkowicz R, Wilezyński M, Wawrzyniak M and Barnaś J 2006 *Phys. Rev.* B **73** 193312
[22] Park H, Park J, Lim A K L, Anderson E H, Alivisatos A P and McEuen P L 2000 *Nature* **407** 57
[23] Wang R Q, Zhou Y Q, Wang B G and Xing D Y 2007 *Phys. Rev.* B **75** 045318
[24] Kikoin K, Kiselev M N and Wegewijs M R 2006 *Phys. Rev. Lett.* **96** 176801
[25] Cornaglia P S, Ness H and Grempel D R 2004 *Phys. Rev. Lett.* **93** 147201
[26] Cornaglia P S, Grempel D R and Ness H 2005 *Phys. Rev.* B **71** 075320
[27] Cornaglia P S and Grempel D R 2005 *Phys. Rev.* B **71** 245326
[28] Koch J and von Oppen F 2005 *Phys. Rev. Lett.* **94** 206804
[29] Koch J, von Oppen F and Andreev A V 2006 *Phys. Rev.* B **74** 205438
[30] Hwang M J, Choi M S and López R 2007 *Phys. Rev.* B **76** 165312
[31] Meir Y and Wingreen N S 1992 *Phys. Rev. Lett.* **68** 2512
[32] Chen Z Z, Lu R and Zhu B F 2005 *Phys. Rev.* B **71** 165324
[33] Mahan G D 2000 *Many-Particle Physics* 3rd edn (New York: Plenum)
[34] Meir Y, Wingreen N S and Lee P A 1991 *Phys. Rev. Lett.* **66** 3048
[35] Wilezyński M, Świrkowicz R and Barnaś J 2006 *Phys. Status Solidi* c **3** 105
[36] Utsumi Y, Martinek J, Schön G, Imamura H and Maekawa S 2005 *Phys. Rev.* B **71** 245116